frontiers | Frontiers in Marine Science

TYPE Original Research
PUBLISHED 06 December 2023
DOI 10.3389/fmars.2023.1255915

OPEN ACCESS

EDITED BY
Satya Panigrahi,
Indira Gandhi Centre for Atomic Research (IGCAR), India

REVIEWED BY
Jelena Godrijan,
Rudjer Boskovic Institute, Croatia
Hyungseok Kim,
Massachusetts Institute of Technology, United States

*CORRESPONDENCE
Qiang Hao
haoq@sio.org.cn

RECEIVED 10 July 2023
ACCEPTED 22 November 2023
PUBLISHED 06 December 2023

CITATION
Zhang W, Hao Q, Zhu J, Deng Y, Xi M, Cai Y, Liu C, Zhai H and Le F (2023) Nanoplanktonic diatom rapidly alters sinking velocity via regulating lipid content and composition in response to changing nutrient concentrations. *Front. Mar. Sci.* 10:1255915. doi: 10.3389/fmars.2023.1255915

Nanoplanktonic diatom rapidly alters sinking velocity via regulating lipid content and composition in response to changing nutrient concentrations

Wei Zhang[1,2,3], Qiang Hao[1,2,4]*, Jie Zhu[1,2,5], Yangjie Deng[1,2], Maonian Xi[1,2], Yuming Cai[1,2], Chenggang Liu[1,2], Hongchang Zhai[1,2] and Fengfeng Le[1,2]

[1]Second Institute of Oceanography, Ministry of Natural Resources, Hangzhou, China, [2]Key Laboratory of Marine Ecosystem Dynamics, Ministry of Natural Resources, Hangzhou, China, [3]Key Laboratory of Nearshore Engineering Environment and Ecological Security of Zhejiang Province, Second Institute of Oceanography, Ministry of Natural Resources, Zhoushan, China, [4]State Key Laboratory of Satellite Ocean Environment Dynamics, Second Institute of Oceanography, Ministry of Natural Resources, Hangzhou, China, [5]Ocean College, Zhejiang University, Zhoushan, China

Diatom sinking plays a crucial role in the global carbon cycle, accounting for approximately 40% of marine particulate organic carbon export. While oceanic models typically represent diatoms as microphytoplankton (> 20 μm), it is important to recognize that many diatoms fall into the categories of nanophytoplankton (2-20 μm) and picophytoplankton (< 2 μm). These smaller diatoms have also been found to significantly contribute to carbon export. However, our understanding of their sinking behavior and buoyancy regulation mechanisms remains limited. In this study, we investigate the sinking behavior of a nanoplanktonic diatom, *Phaeodactylum tricornutum* (*P. tricornutum*), which exhibits rapid changes in sinking behavior in response to varying nutrient concentrations. Our results demonstrate that a higher sinking rate is observed under phosphate limitation and depletion. Notably, in phosphate depletion, the sinking rate of *P. tricornutum* was 0.79 ± 0.03 m d^{-1}, nearly three times that of the previously reported sinking rates for *Skeletonema costatum*, *Ditylum brightwellii*, and *Chaetoceros gracile*. Furthermore, during the first 6 h of phosphate spike, the sinking rate of *P. tricornutum* remained consistently high. After 12 h of phosphate spike, the sinking rate decreased to match that of the phosphate repletion phase, only to increase again over the next 12 hours due to phosphate depletion. This rapid sinking behavior contributes to carbon export and potentially allows diatoms to exploit nutrient-rich patches when encountering increased nutrient concentrations. We also observed a significant positive correlation ($P < 0.001$) between sinking rate and lipid content ($R = 0.91$) during the phosphate depletion and spike experiment. It appears that *P. tricornutum* regulates its sinking rate by increasing intracellular lipid content, particularly digalactosyldiacylglycerol, hexosyl ceramide, monogalactosyldiacylglycerol, and triglycerides. Additionally, *P. tricornutum* replaces phospholipids with more dense membrane sulfolipids, such as sulfoquinovosyldiacylglycerol under

phosphate shortage. These findings shed light on the intricate relationship between nutrient availability, sinking behavior, and lipid composition in diatoms, providing insights into their adaptive strategies for carbon export and nutrient utilization.

KEYWORDS

sinking rate, nutrient limitation, lipid accumulation and remodeling, nanoplanktonic diatom, phaeodactylum tricornutum, biological carbon pump

Introduction

Sinking is a crucial factor influencing the spatial distribution (Smayda, 1970) and vertical carbon flux of phytoplankton in the ocean, as well as their successional patterns and seasonal cycles across different size classes (Bienfang et al., 1982). Among these phytoplankton, diatoms are significant contributors to organic carbon production (Smetacek, 1999), accounting for approximately 20% of Earth's total primary productivity and up to 40% of primary productivity in the oceans (Field et al., 1998). Their sinking behavior plays a critical role in the global carbon cycle, contributing around 40% of the export of particulate organic carbon to the mesopelagic and bathypelagic layers (Jin et al., 2006). However, the specific contributions of different diatom taxa to carbon export remain poorly studied.

Numerous environmental parameters, including temperature, salinity (Bienfang and Szyper, 1982), irradiance (Granata, 1991), and nutrient availability (Bienfang, 1981; Bienfang et al., 1982; Du Clos et al., 2021), significantly impact the sinking rate of diatoms. Nutrients, in particular, are essential for diatom growth and are closely linked to their photosynthetic and physiological status. It is widely recognized that diatoms exhibit lower sinking rates under nutrient-replete conditions. For instance, *Skeletonema costatum*, *Chaetoceros gracile Schütt*, and *Ditylum brightwellii* display significantly higher sinking rates under silicon-limited conditions, while nitrogen and phosphorus limitation reduce their sinking rates (Bienfang et al., 1982). Similarly, *Coscinodiscus wailesii* exhibits higher sinking rates under each of the three nutrient-limited conditions (Du Clos et al., 2021).

Various buoyancy regulation mechanisms have been proposed, primarily based on changes in cell density. These mechanisms include selective ion transport (Anderson and Sweeney, 1978), organic permeates generation (Boyd and Gradmann, 2002), carbohydrate ballast effect (Lavoie et al., 2016), opal accumulation (Turner, 2015; Tréguer et al., 2018), lipid accumulation (Anderson and Sweeney, 1977), active water molecule transport (Raven and Doblin, 2014), and periodic cell expansion (Lavoie and Raven, 2020).

Despite numerous studies investigating changes in diatom sinking rates in response to varying nutrient concentrations and buoyancy regulation mechanisms, most of these studies have focused exclusively on microphytoplanktonic diatoms (> 20 μm). The effects of different nutrient limitations on sinking behavior have not been explored in nanophytoplanktonic diatoms (2-20 μm) and picophytoplanktonic diatoms (< 2 μm). Notably, quasi-monotypic blooms of small diatoms (< 20 μm) have been observed in well-mixed environments at mid- and high-latitudes (Gould and Wiesenburg, 1990; Canovas et al., 1996; Buck et al., 2008; Daniels et al., 2015), with their frustules found in high abundances in sediment trap samples (Leblanc et al., 2018). These tiny diatoms play a crucial role in the microbial loop (Legendre and Le FÃƒÂ¨vre, 1995) and contribute significantly to global carbon export.

Phaeodactylum tricornutum (*P. tricornutum*), a pennate marine diatom, is a valuable model organism that is widely distributed in the marine environment, particularly in the coastal regions of the China Sea (Xue et al., 2018). Under certain environmental conditions, excessive growth of *P. tricornutum* can occur in coastal waters (Cai et al., 2009), exerting a significant impact on the aquatic ecosystem (Liu et al., 2015). In summer, phosphorus limitations are observed in some Chinese estuaries, such as the Yangtze River and Pearl River estuaries, due to high nitrogen and low phosphorus runoff (Wong et al., 1998; Xu et al., 2008). Moreover, the nutrient concentrations in these estuaries and adjacent waters vary spatially and temporally due to the convergence of ocean currents or interactions with the shelf edge (Chen et al., 2012). The effects of nutrient limitations and rapid changes in nutrient concentrations on the sinking rate of *P. tricornutum*, as well as its buoyancy regulation mechanisms, remain unclear.

P. tricornutum exhibits three morphotypes: fusiform, triradiate, and ovate (Lewin et al., 1958; Martino et al., 2007). Compared to typical diatoms, *P. tricornutum* has lower silica content, with only the ovate form possessing a frustule. Figure 1 illustrates the co-dominance of the fusiform and triradiate forms in the experiments. In this study, we investigated changes in the sinking behavior of *P. tricornutum* under nutrient-replete, nutrient-limited, nutrient-depleted, and nutrient-restored conditions using a single culture. We also examined intracellular parameters closely associated with cell density, including lipid, carbohydrate, and protein content and composition. Correlation analysis was applied to investigate the mechanisms underlying the buoyancy regulation of *P. tricornutum*.

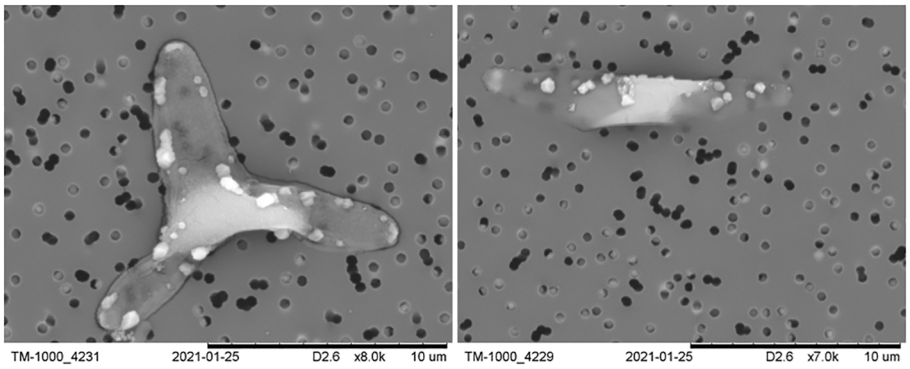

FIGURE 1
The morphotypes of codominant *P. tricornutum* in the present experiments.

Materials and methods

Diatom cultures

The diatom *P. tricornutum* was obtained from Shanghai Guangyu Biological Technology Co., Ltd. It was cultured in sterile natural seawater, supplemented with nutrients, trace metals, and vitamins following the f/2 recipe (Guillard & Ryther, 1962; Orlowska et al., 2017). The culture conditions for *P. tricornutum* included a temperature of 25 °C and a light-dark cycle of 12:12 hours.

Single nutrient depletion and spike experiments

The experiments aimed to analyze the effects of nutrient depletion (PO_4^{3-} and NO_3^-) and subsequent recovery on *P. tricornutum*. To acclimate the cells to the experimental conditions, daily dilutions were performed using sterile natural seawater with consistent nutrient concentrations. This adjustment process lasted 2-3 days before each experiment, ensuring the biomass matched that of the previous day. The cultures were then transferred to glass bottles and diluted to a volume of 15 L with sterile natural seawater, while maintaining an initial cell abundance of approximately 10^5 cells per mL. The initial concentrations of nitrate, phosphate, and silicate for the phosphate-depletion and nitrate-depletion experiments were set at 50 μM, 2 μM, 50 μM, and 12 μM, 10 μM, 50 μM, respectively. Trace metals and vitamins were added based on the f/2 culture media. Throughout the nutrient-depletion experiments, non-limiting nutrients, trace metals, and sufficient vitamins were maintained to ensure only one nutrient became limiting. The strain was cultured under a light intensity of approximately 250 μmol photon m^{-2} s^{-1}, with a 12:12 h light-dark cycle, at room temperature. The culture had a salinity of 28.5‰, a pH of 8.0, and was continuously stirred at 160 rpm. The first light exposure begins at time point zero. In the single nutrient depletion experiment, nutrient samples are collected every 12 hours, and cell abundance and transparent exopolymer particles samples are collected every 24 hours. Nutrient status was determined based on the growth rate of the cells, classified as: (1) nutrient-repletion (NR), representing log-phase growth; (2) nutrient-limitation (NL), with a growth rate of 0.3~0.1 d^{-1}; (3) nutrient-depletion (ND), where the growth rate approached zero. When the growth rate neared zero, the missing nutrient was added to the culture to restore replete conditions. This process is referred to as a nutrient spike. Sinking rate, protein, carbohydrate, total lipid, and absolute quantitative lipidomics analyses were conducted at three nutrient statuses and five time points: nutrient-repletion, nutrient-limitation, nutrient-depletion, and 2, 6, 12, 18, and 24 hours after adding the limiting nutrient.

Growth conditions

Cell abundance was monitored using an automated cell counter from Shanghai RuiYu Biotech Co. Ltd. The growth rate (μ, d^{-1}) was calculated daily using the following Equation 1:

$$\mu = \frac{\ln(C_1/C_0)}{t_1 - t_0} \quad \text{(Eq. 1)}$$

where C_0 and C_1 represent the cell concentrations at times t_0 and t_1, respectively.

The optimal photochemical efficiency of photosystem II (PSII) was measured daily using water pulse amplitude modulated (PAM) fluorometry from Heinz Walz GmbH (91090 Effeltrich, Germany). Prior to measurement, samples underwent a 20-minute dark treatment to obtain F_m (maximum fluorescence) and F_0 (minimum fluorescence). The maximum photosynthetic quenching capacity (F_v) was then calculated as the difference between F_m and F_0.

Nutrient analysis

To analyze the nutrient content, water samples were filtered using 0.45 μm polycarbonate membranes. Thymol spectrophotometry (Osibanjo & Ajayi, 1980), Naphthylethylenediamine hydrochloride

spectrophotometry (Tarafder & Rathore, 1988), molybdenum blue method (Holman, 1943), and silicon molybdenum blue method (Luke, 1953) were employed to measure the concentrations of nitrate, nitrite, phosphate, and silicate, respectively. The total nitrogen concentration was determined by summing the concentrations of nitrite and nitrate.

Sinking rate analysis

The sinking rate of the cells was determined using the SETCOL method outlined by Bienfang (1981). The SETCOL apparatus, as depicted in Figure 2, consisted of three opaque plastic columns measuring 1.0 m in length and with a volume of 1111 mL. Each column was filled with a homogeneous water sample efficiently. Following this, the columns were left undisturbed at room temperature for 3 hours. Precipitated samples were collected from the bottom, middle, and upper compartments of the columns by sequential drainage. The phytoplankton biomass in each compartment was determined by measuring chlorophyll-*a* concentration (Chl-*a*), and the sinking rate was calculated using the following Equation 2:

$$\theta = ({}^{B_s}/_{B_t}) \times {}^{L}/_{t} \quad \text{(Eq. 2)}$$

where θ represents the sinking rate in meters per day (m d^{-1}), B_s denotes the biomass settled into the bottom compartment, B_t indicates the total biomass in the column, L signifies the column length in meters, and t represents the settling time in days.

For Chl-*a* analysis, the samples were filtered using 25 mm GF/F filters with a pore size of 0.65 μm under low vacuum pressure (< 0.04 MPa). Subsequently, the filtered samples were stored in the dark at -20 °C. After 24 hours of extraction with 90% acetone at -20° C, the Chl-*a* concentration was measured using a Turner-Designs Trilogy™ fluorometer (Caspers, 1970).

Transparent exopolymer particles (TEPs) analysis

Concentrations of TEPs were measured using a modified version of a previously established method (Passow and Alldredge, 1995). Triplicate 10 mL samples were filtered through 0.4 μm pore size polycarbonate filters under a low constant vacuum (< 0.02 MPa). The filters were then stained with 0.5 mL of a 0.02% Alcian Blue solution for 2 seconds. To eliminate excess dye, the filters were rinsed twice with 2 mL of distilled water. Next, the filters were subjected to an extraction process using 6 mL of 80% sulfuric acid for 2 hours. The absorbance of TEPs was determined at 787 nm using a spectrophotometer, with Xanthan gum serving as the standard.

Cell physiological and biochemical analysis

The cell morphology was analyzed using a scanning electron microscope (Model: TM-1000 Tabletop Microscope, company:

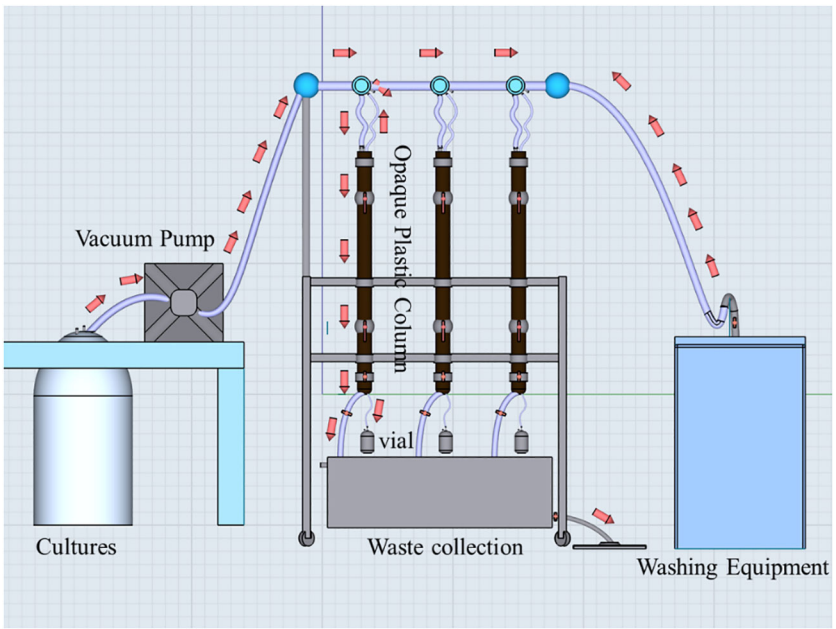

FIGURE 2
The SETCOL apparatuses. The red arrows indicate the direction of liquid flow. Initially, the algal suspension was introduced into three opaque plastic columns using a vacuum pump. Once all three columns were filled, the vacuum pump and the bottom valve of each column were closed. Subsequently, the columns were left undisturbed at room temperature for a period of 3 hours. Following this, the two valves located in the middle and upper sections of each column were closed, and sequential samples were collected from the bottom, middle, and top sections of each column. Chl-*a* concentrations in these samples, as well as the initial algal suspension, were measured to calculate the sinking rate of microalgae. After completing the experiment, the three columns were rinsed with distilled water five times and prepared for future use.

Hitachi High-Technologies Corporation). To prepare the samples, 10 mL aliquots were filtered through 3.0 µm pore size isopore membrane filters and dried overnight. Subsequently, the filters were placed in a gold injector (Model: MSP-1S, company: Vacuum Device Inc) and coated with a thin layer of gold. Finally, the filters were subjected to scanning electron microscopy for photography.

Prior to protein, carbohydrate, and total lipid analysis, a pre-treatment process was applied to the algal sample. In brief, approximately 3 L of *P. tricornutum* cultures were passed through 0.4 µm pore size polycarbonate filters and washed thrice with distilled water. The filtered *P. tricornutum* cells were then dried at -70 °C under vacuum for 24 hours. Cell disruption was achieved through repeated freeze-thaw cycles. The cells were frozen below -20°C and subsequently thawed at approximately 4°C, repeating this process 3-4 times. This method utilized the formation of intracellular ice particles and the increased concentration of cytosolic salts to induce cell lysis and fragmentation.

Total lipids were extracted and quantified following the protocol described by Johnson and Wen (Johnson and Wen, 2009). Carbohydrate content was determined using the anthrone colorimetric technique as outlined in Laurentin and Edwards (Laurentin and Edwards, 2003). Protein quantitation was performed using the Lowry method (Waterborg, 2009).

Absolute quantitative lipidomics measurement

Triplicate samples were obtained from the cultures during the phosphate depletion and spike experiment. *P. tricornutum* cultures (~50 mL) were filtered through 25 mm diameter 0.2 µm hydrophilic Durapore filters, rinsed thrice with distilled water, and immediately flash-frozen and stored at -80 °C. Lipids were extracted from the filters using the methyl tert-butyl ether (MTBE) method (Matyash et al., 2008). Briefly, the filters were thawed at 4°C and mixed with 200 µL water, 240 µL methanol, and 800 µL MTBE. The mixture was sonicated at low temperature (30 min/once, twice). After centrifugation at 14000 g for 15 min at 10°C, the upper layer was collected and dried under nitrogen.

To analyze the lipids, ultra-high performance liquid chromatography (UHPLC) mass spectrometry (MS) was performed using an UHPLC Nexera LC-30A (SHIMADZU, Japan) coupled to a Q-Exactive Plus high-resolution mass spectrometer (ThermoFisher Scientific, Waltham, MA, USA), following a previously reported method (Liu et al., 2022). Reverse-phase chromatography was employed for LC separation with a CSH C18 column (1.7 µm, 2.1 × 100 mm; Waters). The lipid extracts were re-dissolved in 200 µL of 90% isopropanol/acetonitrile, centrifuged at 14000 g for 15 min, and finally, 3 µL of the sample was injected.

The mobile phase consisted of acetonitrile–water (6:4, vol/vol) with 0.1% formic acid and 0.1 mM ammonium formate as solvent A, and acetonitrile–isopropanol (1:9, vol/vol) with 0.1% formic acid and 0.1 mM ammonium formate as solvent B. The initial mobile phase composition was 30% solvent B at a flow rate of 300 µL/min. It was maintained for 2 min, followed by a linear increase to 100% solvent B over 23 min, and then equilibrated at 5% solvent B for 10 min. Mass spectra were acquired using the Q-Exactive Plus in both positive and negative modes. The Electron Spray Ionization (ESI) parameters were optimized and preset for all measurements: source temperature at 300°C, the capillary temperature at 350°C, ion spray voltage at 3000 V, S-Lens RF Level at 50%, and the scan range set at 200–1800 m/z. For each full scan, 10 fragments (MS2scan, HCD) were collected. The resolution of MS1 was set at 70000 at m/z 200, and that of MS2 was set at 17500 at m/z 200.

To extract and identify the peaks of lipid molecules and internal standard lipid molecules, Lipidsearch (ThermoFisher Scientific, USA) was utilized. The main parameters were as follows: precursor tolerance: 5 ppm, product tolerance: 5 ppm, and product ion threshold: 5%. The raw data and the lipid category naming explanation for the absolute quantification lipidomics in the phosphate depletion and spike experiment are provided in Table S1 and Data Sheet 1 in the Supplementary Material, respectively.

Data analysis

A Pearson correlation and one-way ANOVA were conducted using IBM SPSS Statistics 22.0 to examine the correlation between sinking rate and detecting parameters (F_v/F_m, growth rate, protein, lipids, carbohydrate, and TEPs) in the nutrient depletion and spike experiments, as well as to determine the differences in each parameter under different nutrient regimes. Significance was determined by ANOVA probabilities< 0.05. The normal distribution of the data was checked first, and log10 transformation was applied if necessary. For data that could not be transformed into a normal distribution, the Spearman correlation and the nonparametric Kruskal-Wallis ANOVA were employed. Data visualization was performed using the R programming language.

Results

P. tricornutum was acclimatized to the initial nutrients for 2 days before the nutrient-limitation experiments. The initial cell abundances were 2.34×10^5 and 1.05×10^5 cell ml^{-1} for phosphate and nitrate limitation, respectively. Figure 3 presents the cell abundance and growth rate data for these two experiments, while Figure 4 displays the limiting-nutrient concentrations and sinking rate data. The optimal photochemical efficiency of photosystem II (F_v/F_m), cellular contents (protein, carbohydrate, and lipid), and TEPs data are shown in Figures 5–7, respectively. The sinking rate, as well as the cell physiological and biochemical responses to nutrient depletion and spike, will be addressed separately below.

Phosphate depletion and spike experiment

During the initial 72 hours of the experiment, *P. tricornutum* exhibited log-phase growth as a result of phosphate repletion (PR). The growth rate (Figure 3A) and F_v/F_m (Figure 5) initially increased

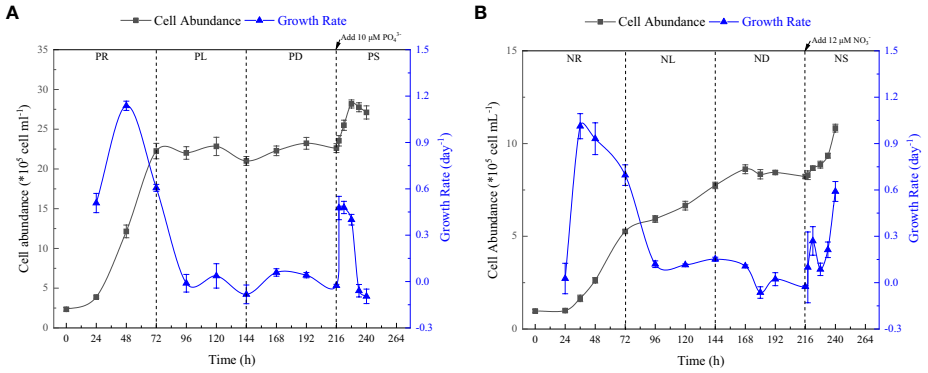

FIGURE 3
Cell abundance and growth rate data for phosphate depletion-spike experiment **(A)** and nitrate depletion-spike experiment **(B)**. PR, PL, PD, and PS represent phosphate repletion, phosphate limitation, phosphate depletion, and phosphate spike, respectively. NR, NL, ND, and NS represent nitrate repletion, nitrate limitation, nitrate depletion, and nitrate spike, respectively. These abbreviations apply to all figures.

but subsequently decreased. The mean values for the growth rate and F_v/F_m were 0.75 ± 0.34 d^{-1} and 0.52 ± 0.04, respectively. *P. tricornutum* rarely settled during the PR phase, with a mean sinking rate of -0.06 ± 0.13 m d^{-1} (Figure 4A). While the intracellular total lipid content remained stable, the protein and carbohydrate contents fluctuated (Figure 6A). The mean total lipid content was 0.16 ± 0.01 mg mg^{-1}. Throughout the PR phase, the concentration of TEPs consistently increased (Figure 7).

After 72 hours of PR, the extracellular phosphate was depleted (Figure 4A), resulting in a significant decline in the growth rate and F_v/F_m to values of -0.08 ± 0.06 d^{-1} and 0.37 ± 0.01, respectively. This indicated that *P. tricornutum* faced constraints due to limited phosphate availability and reduced photosynthetic efficiency. Additionally, the sinking speed significantly increased from -0.21 ± 0.08 to 0.58 ± 0.10 m d^{-1} ($P< 0.05$). Under phosphate limitation (PL) conditions, there was minimal variation observed in carbohydrate and TEPs, while the protein concentration slightly decreased. Notably, the total lipid content significantly ($P< 0.05$) increased from 0.15 ± 0.01 to 0.25 ± 0.01 mg mg^{-1}.

In the phosphate depletion phase (PD), following 72 hours of PL, the growth rate exhibited fluctuating increases, rising from -0.08 ± 0.06 to -0.03 ± 0.01 d^{-1} (Figure 3A). This fluctuation in growth rate could potentially be attributed to the re-release of restricted nutrients through cell fragmentation. Moreover, the sinking rate, total lipid content, and TEPs consistently increased, while the concentrations of protein and carbohydrate decreased.

Subsequent to the PD phase, a phosphate spike (PS) experiment was conducted. After the first 2 hours following the phosphate spike (R2h), both the growth rate and F_v/F_m significantly increased ($P< 0.05$). The growth rate rose from -0.03 ± 0.01 to 0.48 ± 0.08 d^{-1}, while the F_v/F_m increased from 0.34 ± 0.01 to 0.47 ± 0.01. However, after 6 hours following the PS (R6h), both the growth rate and F_v/F_m began to continuously decline. Furthermore, after 18 hours of phosphate recovery treatment (R18h), the growth rate decreased to -0.06 ± 0.04 d^{-1}, indicating a re-imposition of phosphate limitation on *P. tricornutum*. The sinking rate and total lipid content initially decreased, then increased during the PS phase. In contrast, the concentration of TEPs showed an initial increase

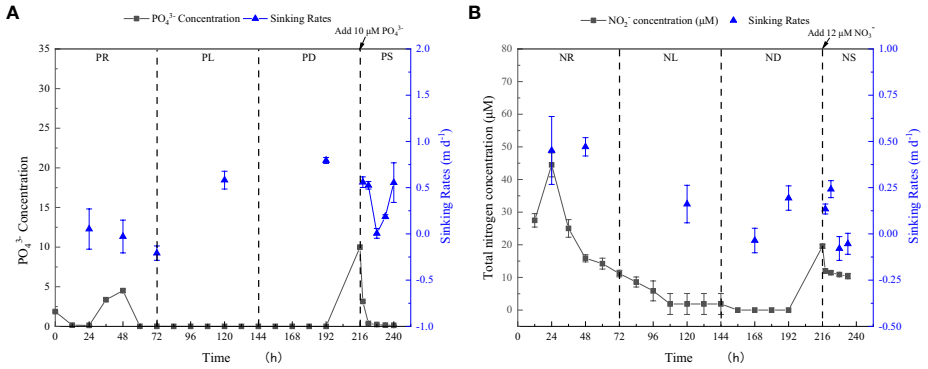

FIGURE 4
Limiting-nutrient concentrations and sinking rate data for phosphate depletion-spike experiment **(A)** and nitrate depletion-spike experiment **(B)**. The total nitrogen concentration is the sum of nitrite and nitrate concentrations.

10.3389/fmars.2023.1255915

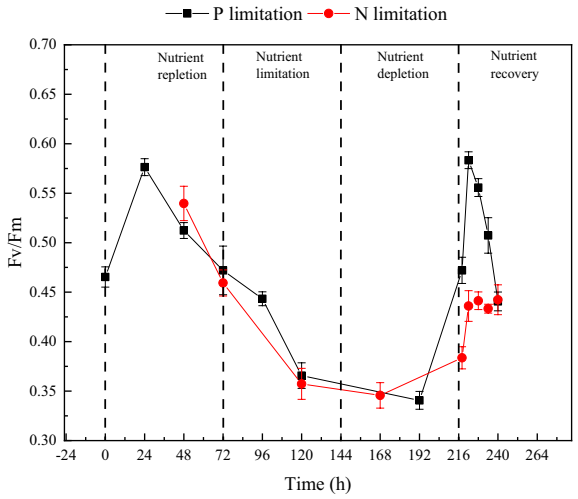

FIGURE 5
The changes in optimal photochemical efficiency of photosystem II (F_v/F_m) throughout the phosphate depletion-spike experiment (black square) and nitrate depletion-spike experiment (red circle).

followed by a subsequent decrease. After 12 hours of phosphate recovery (R12h), the sinking rate and total lipid content reached their lowest values of 0.01 ± 0.05 m d^{-1} and 0.16 ± 0.02 mg mg^{-1}, respectively. However, with the re-imposition of phosphate limitation, the sinking rate and total lipid content increased again. The concentrations of protein and carbohydrates exhibited fluctuating changes during the phosphate recovery period.

Nitrate depletion and spike experiment

Compared to the phosphate depletion experiment, the nitrate depletion experiment showed similar trends in cell abundance, growth rate, F_v/F_m, and TEPs variations. During the initial stage of the experiment (nitrate repletion, NR) from 0 to 72 hours, there was a rapid increase in cell abundance and TEPs, while the growth rate, settling rate, and F_v/F_m remained high. After 72 hours of nitrate sufficiency, the growth rate of *P. tricornutum* significantly decreased ($P< 0.05$) from 0.70 ± 0.07 to 0.12 ± 0.02 d^{-1} (Figure 3B). Simultaneously, the F_v/F_m value declined from 0.46 ± 0.01 to 0.36 ± 0.02 (Figure 5), indicating nitrate limitation (NL) in *P. tricornutum*. The sinking rate decreased to 0.16 ± 0.10 m d^{-1}, one-third of the rate under nitrate-replete conditions (Figure 4B). Under NL conditions, protein concentration (Figure 6B) and TEPs (Figure 7) remained almost unchanged, while total lipid concentration slightly decreased. However, carbohydrate content significantly ($P< 0.05$) increased from 2.00 ± 0.14 to 7.04 ± 0.46 mg mg^{-1}.

After 72 hours of NL, the total nitrogen concentration and growth rate approached zero, marking the beginning of nitrogen depletion (ND). The sinking rate and intracellular content concentrations were within the range of measured values during NL. The TEPs concentration increased from 21.31 ± 0.05 × 10^3 to 26.01 ± 10.99 × 10^3 μg Xeq. L^{-1}.

In the first 6 hours after the nitrate spike (NS), from 216 to 222 hours, the growth rate and F_v/F_m had regained values typical of the nitrate-replete state. The sinking rate of *P. tricornutum* exhibited a slight fluctuating increase, and the TEPs concentration slightly increased during this time. Between 6 and 24 hours after the NS, *P. tricornutum* continued to show log-phase growth while maintaining relatively high values of F_v/F_m. However, the sinking rate decreased from 0.24 ± 0.05 to -0.05 ± 0.06 m d^{-1}. The intracellular contents and TEPs concentrations showed fluctuating changes during the NS period.

Relationship between sinking rate and physiological-biochemical parameters in the nutrient depletion and spike experiments

Figure 8A shows the correlations between sinking rate and physiological-biochemical parameters in phosphate depletion and spike experiments. The correlation plots reveal a significant positive

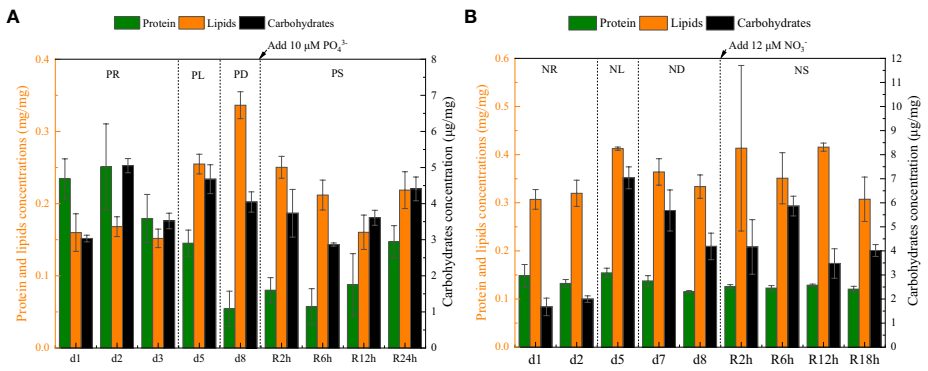

FIGURE 6
The intracellular contents (protein, carbohydrate, and lipid) data for phosphate depletion and spike experiment **(A)** and nitrate depletion and spike experiment **(B)**.

10.3389/fmars.2023.1255915

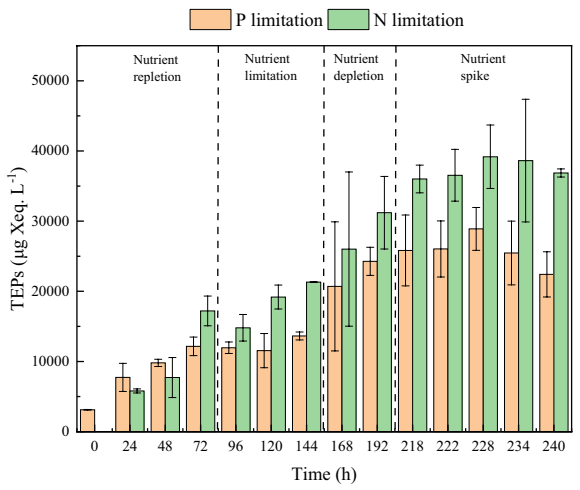

FIGURE 7
The TEPs concentrations in the phosphate depletion-spike experiment (orange pillar) and nitrate depletion-spike experiment (green pillar).

relationship (P< 0.001) between sinking rate and lipid content (R = 0.91). Conversely, lipid content demonstrates a significant negative correlation (P< 0.05) with F_v/F_m (R = -0.77). Additionally, TEPs concentration exhibits a significant (P< 0.01) negative linear relationship (R = -0.89) with protein content.

In Figure 8B, the correlations among parameters in nitrate depletion and spike experiments are presented. The results demonstrate significant positive associations (P< 0.01) between F_v/F_m and growth rate (R = 0.85). Furthermore, TEPs show significant negative correlations (P< 0.05) with protein content (R = -0.60) and sinking rate (R = -0.71). The carbohydrate concentration exhibits significant negative correspondences (P< 0.05) with F_v/F_m (R = -0.81).

Cell aggregation in the phosphate depletion and spike experiments

Figure 9 illustrates the overall cell population morphology in the four phosphate phases. In instances where phosphate was restricted and depleted, there was an enhancement in cell aggregation, resulting in a significant increase in the number of aggregates. However, within 24 hours after the phosphate spike, the number of cell aggregates decreased.

Lipid remodeling in the phosphate depletion and spike experiments

In the experiments involving phosphate depletion and spike, a significant correlation was observed between the settling rate and total lipid content. To further understand the buoyancy regulation mechanism of *P. tricornutum*, lipidomics analysis was conducted on the seven phases (PR, PL, PD, R2h, R6h, R12h, and R24h) of the phosphate depletion and spike experiment, and the findings are presented in Table 1. The lipid composition of *P. tricornutum* mainly consists of glycerophospholipids, glycerolipids, serol lipids, sphingolipids, saccharolipids, prenol lipids, and fatty acyls. Among these, glycerophospholipids, glycerolipids, sphingolipids, and saccharolipids exhibited higher abundances. During the transition from PR to PL and PD, the content of glycerolipids and saccharolipids gradually increased, particularly in subclasses such as triglyceride (TG), digalactosyldiacylglycerol (DGDG), monogalactosyldiacylglycerol (MGDG), and sulfoquinovosyldiacylglycerol (SQDG). However, during the phosphate spike (PS) phase, the content of these lipids gradually decreased until 24 hours after PS, when their content began to rise again. Furthermore, subclasses such as phosphatidylinositol (PI) in glycerophospholipids and hexosylceramide (Hex1Cer) in sphingolipids exhibited similar trends of variation as these lipids.

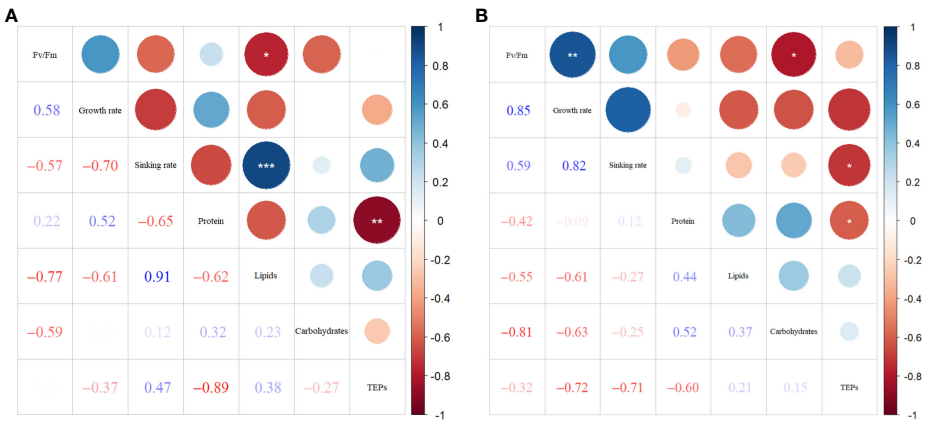

FIGURE 8
Correlation plots of sinking rate with physiological-biochemical parameters in phosphate depletion-spike experiment **(A)**, and nitrate depletion-spike experiment **(B)**. *: P< 0.05; **: P< 0.01; ***: P< 0.001. .

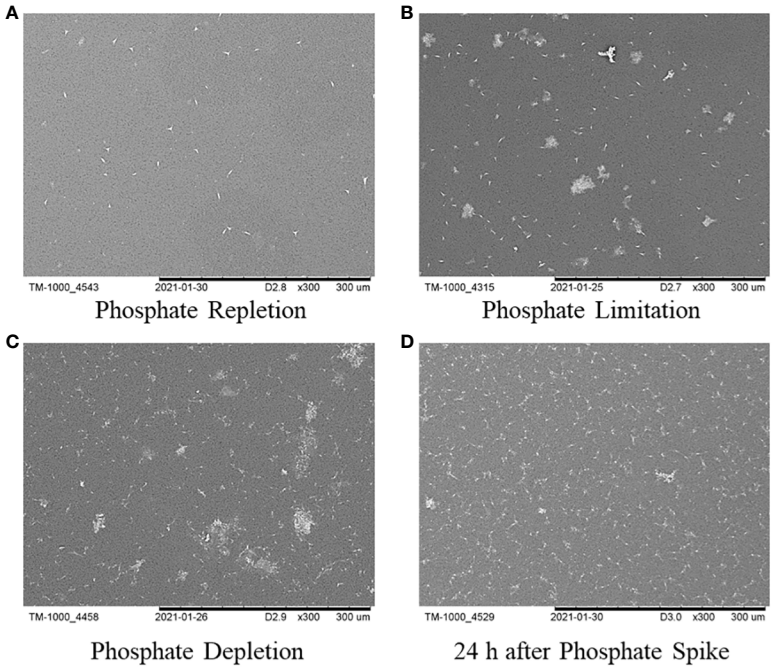

FIGURE 9
The overall cell population morphology of *P. tricornutum* in the four time points: **(A)** phosphate repletion; **(B)** phosphate limitation; **(C)** phosphate depletion; **(D)** 24h after phosphate spike.

Figure 10 illustrates the correlations between the sinking rate and lipid subclasses during the phosphate depletion and spike experiments. The sinking rate demonstrated significant positive correlations with TG ($R = 0.89$, $P < 0.01$), cholesterol ester (ChE, $R = 0.88$, $P < 0.01$), stigmasterol ester (StE, $R = 0.89$, $P < 0.01$), Hex1Cer ($R = 0.93$, $P < 0.01$), phytosphingosine (phSM, $R = 0.82$, $P < 0.05$), DGDG ($R = 0.86$, $P < 0.05$), MGDG ($R = 0.81$, $P < 0.05$), coenzyme Q (Co, $R = 0.94$, $P < 0.01$), and fatty acid (FA, $R = 0.91$, $P < 0.01$).

Discussion

It is widely acknowledged that nutrient concentration affects the sinking rate of phytoplankton. However, most studies have focused on investigating the response of large diatoms (> 20 μm) (Bienfang et al., 1982; Gemmell et al., 2016; Du Clos et al., 2019) to variations in nutrient concentration, neglecting the impact on nanophytoplankton (2-20 μm) sinking behavior, which plays a crucial role in nearshore carbon export (Gould and Wiesenburg, 1990; Boyd and Newton, 1995; Buck et al., 2008). Consequently, the buoyancy regulation mechanisms of nanophytoplankton remain poorly understood.

Our experiments on *P. tricornutum* revealed that a higher phytoplankton sinking rate was consistently associated with phosphate limitation or depletion. During the first 6 hours of phosphate spike, the sinking rate remained consistently high. However, after 12 hours of phosphate spike treatment, the sinking rate decreased to that observed during the phosphate repletion phase. Similar experimental results were also found in *Coscinodiscus wailesii* (Du Clos et al., 2021). When the ambient nutrient concentration increases suddenly, *P. tricornutum* may maintain a high sinking rate, thereby increasing nutrient flux. Once the internal nutrient reserves of *P. tricornutum* have replenished, it may decelerate its sinking rate, maximizing exposure to light and avoiding additional energy expenditure associated with sinking.

Under phosphate-limited conditions, *P. tricornutum* may control its sinking rate by regulating intracellular lipid content and composition. The sinking rate and lipid content exhibited a simultaneous increase and decrease, respectively, during the phosphate depletion and spike experiment. There was a significant ($P < 0.001$) positive correlation ($R = 0.91$) between the sinking rate of *P. tricornutum* and lipid content, consistent with the findings of Alipanah et al. (2018).

The limitation and depletion of phosphate not only increased the content of lipids but also altered their composition. Glycerophospholipids and saccharolipids were found to be essential components of the photosynthetic membranes (thylakoid lipidome) in phytoplankton (Boudière et al., 2014). The envelopes and thylakoid membranes of *P. tricornutum* chloroplasts primarily consisted of the following lipids (Table 1): 1) glycerophospholipids - phosphatidylcholine (PC), phosphatidylethanolamine (PE), phosphatidylglycerol (PG), and phosphatidylinositol (PI); 2) saccharolipids - MGDG, DGDG, and SQDG. When phosphate was scarce in the environment, a shortage of phosphate triggered an increase in the content of saccharolipids within the chloroplast, potentially contributing to phosphate storage. Additionally, the limitation or depletion of phosphate resulted in elevated levels of TG and Hex1Cer in *P. tricornutum*. A significant ($P < 0.05$) positive correlation was

10.3389/fmars.2023.1255915

TABLE 1 The lipid composition and content (mg g^{-1}) in the seven phases of the phosphate depletion and spike experiment: A) phosphate repletion (PR); B) phosphate limitation (PL); C) phosphate depletion (PD); D) 2h after phosphate spike (R2h); E) 6h after phosphate spike (R6h); F) 12h after phosphate spike (R12h); G) 24h after phosphate spike (R24h).

Lipid Group	Class	PR	PL	PD	R2h	R6h	R12h	R24h
Glycerophospholipids	CL	11.1 ± 0.9	5.4 ± 1.4	12.0 ± 1.1	7.8 ± 2.0	11.2 ± 1.4	6.0 ± 1.6	6.6 ± 0.9
	LPC	3.3 ± 0.7	6.9 ± 1.5	1.7 ± 0.4	1.9 ± 0.4	5.2 ± 1.1	2.6 ± 0.6	2.3 ± 0.5
	LPE	0.1 ± 0.0	0.1 ± 0.0	0.0 ± 0.0	0.0 ± 0.0	0.0 ± 0.0	0.0 ± 0.0	0.0 ± 0.0
	LPG	0.1 ± 0.0	0.1 ± 0.0	0.0 ± 0.0	0.1 ± 0.0	0.1 ± 0.0	0.1 ± 0.0	0.0 ± 0.0
	PA	1.4 ± 0.3	1.1 ± 0.2	1.1 ± 0.0	0.8 ± 0.2	0.8 ± 0.2	0.4 ± 0.1	0.7 ± 0.2
	PC	2.6 ± 0.6	2.6 ± 0.5	3.2 ± 0.7	2.7 ± 0.6	3.6 ± 0.8	1.6 ± 0.3	1.8 ± 0.4
	PE	2.0 ± 0.4	1.3 ± 0.3	1.2 ± 0.3	1.0 ± 0.2	1.2 ± 0.3	0.7 ± 0.1	0.8 ± 0.2
	PG	16.2 ± 0.7	8.3 ± 0.8	8.3 ± 1.3	20.4 ± 2.4	16.5 ± 1.0	11.3 ± 1.5	7.8 ± 1.2
	PI	19.4 ± 2.1	29.7 ± 2.8	35.2 ± 0.5	23.8 ± 2.0	17.4 ± 1.8	13.9 ± 1.6	18.4 ± 1.9
	PIP	0.2 ± 0.0	1.1 ± 0.2	0.8 ± 0.2	0.6 ± 0.1	0.5 ± 0.1	0.3 ± 0.1	0.3 ± 0.1
	PIP2	0.1 ± 0.0	0.0 ± 0.0	0.1 ± 0.0	0.1 ± 0.0	0.0 ± 0.0	0.0 ± 0.0	0.0 ± 0.0
	PS	0.5 ± 0.1	1.3 ± 0.3	0.9 ± 0.2	0.6 ± 0.1	0.6 ± 0.1	0.3 ± 0.1	0.4 ± 0.1
	Total	56.9 ± 5.6	57.8 ± 7.9	64.6 ± 4.3	59.7 ± 4.7	57.0 ± 6.7	37.1 ± 5.8	39.4 ± 5.4
Glycerolipids	DG	5.3 ± 1.1	2.7 ± 0.7	4.1 ± 0.9	2.5 ± 0.6	2.9 ± 0.6	1.6 ± 0.4	2.7 ± 0.6
	MG	0.1 ± 0.0	0.1 ± 0.0	0.1 ± 0.0	0.1 ± 0.0	0.1 ± 0.0	0.1 ± 0.0	0.1 ± 0.0
	TG	30.5 ± 1.7	107.8 ± 3.2	160.1 ± 7.4	104.4 ± 7.3	80.2 ± 6.7	69.3 ± 10.2	102.9 ± 14.9
	Total	35.9 ± 2.7	110.6 ± 3.8	164.3 ± 7.8	107.0 ± 7.8	83.2 ± 7.2	71.0 ± 10.7	105.7 ± 15.3
Serol lipids	ChE	0.1 ± 0.0	0.1 ± 0.0	0.1 ± 0.0	0.1 ± 0.0	0.1 ± 0.0	0.1 ± 0.0	0.1 ± 0.0
	StE	0.2 ± 0.0	0.5 ± 0.1	0.5 ± 0.1	0.5 ± 0.1	0.3 ± 0.1	0.3 ± 0.1	0.3 ± 0.1
	Total	0.2 ± 0.1	0.5 ± 0.1	0.6 ± 0.2	0.5 ± 0.1	0.4 ± 0.1	0.3 ± 0.1	0.4 ± 0.1
Sphingolipids	Cer	1.0 ± 0.2	0.5 ± 0.1	1.0 ± 0.2	0.5 ± 0.1	0.9 ± 0.2	0.3 ± 0.1	0.6 ± 0.1
	CerG2GNAc1	0.4 ± 0.1	0.3 ± 0.1	0.5 ± 0.1	0.2 ± 0.1	0.3 ± 0.1	0.2 ± 0.0	0.3 ± 0.1
	CerP	0.1 ± 0.0	0.1 ± 0.0	0.1 ± 0.0	0.1 ± 0.0	0.2 ± 0.0	0.0 ± 0.0	0.1 ± 0.0
Sphingolipids	GM3	0.2 ± 0.0	0.1 ± 0.0	0.1 ± 0.0	0.1 ± 0.0	0.1 ± 0.0	0.1 ± 0.0	0.1 ± 0.0
	Hex1Cer	11.3 ± 1.1	21.4 ± 1.1	24.6 ± 1.0	19.4 ± 1.3	15.5 ± 0.8	11.4 ± 2.0	17.4 ± 1.7
	Hex2Cer	0.7 ± 0.2	0.5 ± 0.1	0.6 ± 0.1	0.4 ± 0.1	0.8 ± 0.2	0.3 ± 0.1	0.5 ± 0.1
	Hex3Cer	0.1 ± 0.0	0.1 ± 0.0	0.1 ± 0.0	0.0 ± 0.0	0.0 ± 0.0	0.0 ± 0.0	0.0 ± 0.0
	phSM	0.0 ± 0.0	0.3 ± 0.1	0.4 ± 0.1	0.3 ± 0.1	0.3 ± 0.1	0.2 ± 0.0	0.2 ± 0.1
	SM	0.1 ± 0.0	0.1 ± 0.0	0.1 ± 0.0	0.1 ± 0.0	0.1 ± 0.0	0.1 ± 0.0	0.1 ± 0.0
	SPH	16.3 ± 1.0	3.0 ± 0.6	2.4 ± 0.6	6.7 ± 0.5	7.6 ± 2.1	1.5 ± 0.3	4.2 ± 0.4
	ST	1.6 ± 0.4	0.3 ± 0.1	0.2 ± 0.1	0.2 ± 0.0	0.2 ± 0.1	0.1 ± 0.0	0.1 ± 0.0
	Total	30.6 ± 2.8	26.1 ± 2.0	29.0 ± 1.5	27.4 ± 2.1	25.1 ± 3.1	14.0 ± 2.5	23.0 ± 2.4
Saccharolipids	DGDG	10.6 ± 0.8	16.3 ± 2.7	23.1 ± 4.3	17.0 ± 1.9	12.6 ± 1.2	9.6 ± 2.4	14.0 ± 1.1
	DGMG	0.4 ± 0.1	0.6 ± 0.1	0.1 ± 0.0	0.1 ± 0.0	0.3 ± 0.1	0.1 ± 0.0	0.1 ± 0.0
	MGDG	14.5 ± 1.6	19.1 ± 1.0	28.1 ± 2.0	20.5 ± 0.7	16.2 ± 1.0	14.6 ± 0.6	18.7 ± 1.5
	MGMG	1.0 ± 0.2	0.9 ± 0.2	0.3± 0.1	0.2 ± 0.0	0.4 ± 0.1	0.3 ± 0.1	0.3 ± 0.1
	SQDG	17.1 ± 0.7	20.2 ± 1.0	23.3 ± 4.8	15.3 ± 0.8	13.8 ± 1.0	11.3 ± 1.4	14.7 ± 0.6
	SQMG	0.5 ± 0.1	0.9 ± 0.2	0.5 ± 0.1	0.7 ± 0.1	1.1 ± 0.3	0.8 ± 0.2	0.6 ± 0.2

(Continued)

TABLE 1 Continued

Lipid Group	Class	PR	PL	PD	R2h	R6h	R12h	R24h
	Total	44.0 ± 2.9	57.9 ± 4.0	75.4 ± 7.2	53.8 ± 2.0	44.4 ± 3.5	36.8 ± 4.5	48.4 ± 2.8
Prenol lipids	Co	0.2 ± 0.0	0.8 ± 0.2	1.4 ± 0.3	1.0 ± 0.2	1.0 ± 0.2	0.5 ± 0.1	1.1 ± 0.2
Fatty Acyls	FA	0.2 ± 0.0	1.0 ± 0.2	0.9 ± 0.2	0.8 ± 0.2	0.7 ± 0.1	0.5 ± 0.1	0.7 ± 0.2
	WE	0.0 ± 0.0	0.0 ± 0.0	0.1 ± 0.0	0.1 ± 0.0	0.1 ± 0.0	0.0± 0.0	0.1 ± 0.0
	Total	0.2 ± 0.0	1.0 ± 0.2	1.0 ± 0.2	0.9 ± 0.2	0.8 ± 0.2	0.5 ± 0.1	0.8 ± 0.2
Total		169.1 ± 14.1	255.4 ± 14.0	337.5 ± 19.7	250.8 ± 15.5	212.9 ± 20.9	160.7 ± 23.9	219.4 ± 25.6

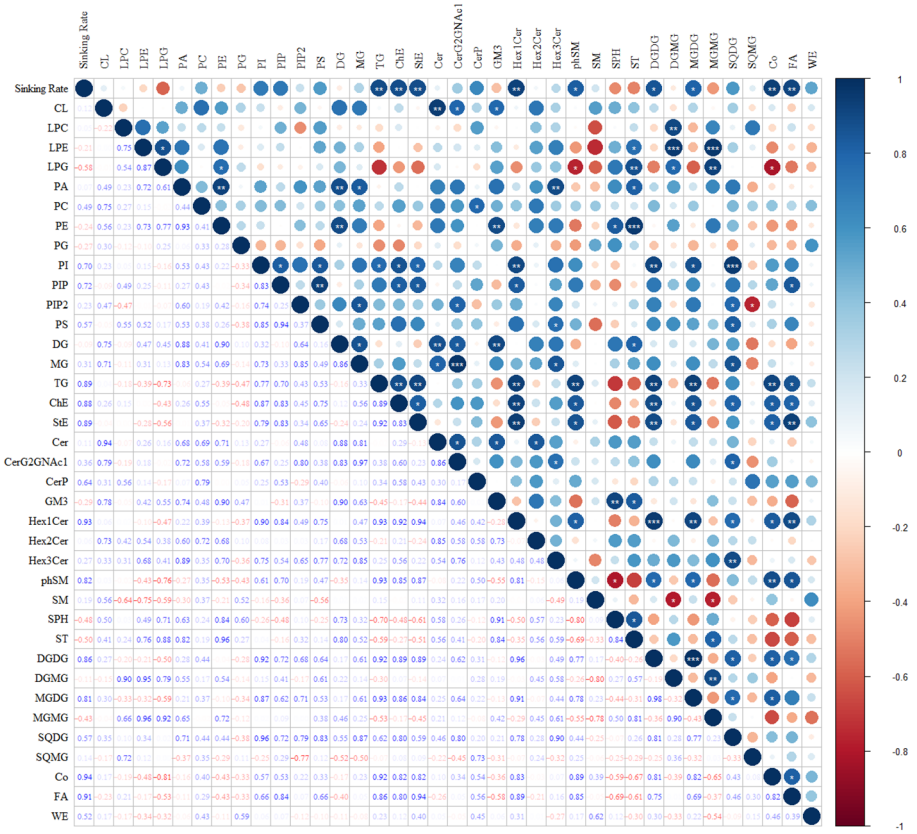

FIGURE 10
The correlations between sinking rate and subclasses of lipids during the phosphate depletion and spike experiments. *: P< 0.05; **: P< 0.01; ***: P< 0.001.

observed between the sinking rate of *P. tricornutum* and the concentration of MGDG, DGDG, TG, and Hex1Cer, which exhibited relatively higher levels. Therefore, under conditions of phosphate limitation, *P. tricornutum* may regulate its sinking rate by altering the levels of MGDG, DGDG, TG, and Hex1Cer.

Furthermore, *P. tricornutum* may modulate its sinking rate by substituting denser sulfolipids for phospholipids. In response to phosphate scarcity, *P. tricornutum* reduced its cellular demand for phosphate by substituting PG with SQDG. PG is an essential phospholipid in photosynthetic membranes due to its role as a cofactor in the photosystems (Alipanah et al., 2018). The sulfolipid SQDG partially fulfills the functions of PG during phosphate limitation (Van Mooy et al., 2009). From phosphate repletion to phosphate depletion, there was a significant increase in the ratio of SQDG to PG in *P. tricornutum*, rising from 1.1 ± 0.2 to 2.8 ± 0.4 (Table 2). This phenomenon has been commonly observed in cyanobacteria and eukaryotic phytoplankton such as *Synechococcus*, *Prochlorococcus*, *Crocosphaera watsonii*, *Trichodesmium erythreum*, *Thalassiosira pseudonana*, and *Chaetoceros affinis* (Table 2).

Comparing the physiological and biochemical analysis of the nitrate and phosphate depletion and spike experiments, similar and unique regulations were identified. In both experiments, the photosynthetic capacity initially decreased during nutrient depletion and then increased after nutrient spike. However, a renewed and sustained reduction in photosynthetic capacity occurred only after 6 hours of phosphate spike treatment. Moreover, after 24 hours of phosphate spike treatment, the photosynthetic capacity, growth rate, and sinking rate returned to

TABLE 2 Ratios of sulfolipid to phospholipids (SQDG/PG) in phytoplankton cultures.

	SQDG/PG, P-replete	SQDG/PG, P-deplete	
Cyanobacteria			
Synechococcus WH8102	9.9 ± 2.0	120.5 ± 7.1	Mooy et al.
Synechococcus WH7803	10.3 ± 0.3	61.6 ± 15.4	Mooy et al.
Synechococcus WH5701	6.2 ± 0.5	132.0 ± 31.0	Mooy et al.
Prochlorococcus MED4	20.0 ± 1.3	34.1 ± 1.6	Mooy et al.
Crocosphaera watsonii	4.0	5.8	Mooy et al.
Trichodesmium erythreum	7.8 ± 1.0	18.5 ± 4.9	Mooy et al.
Eukaryotic phytoplankton			
Thalassiosira pseudonana	3.0 ± 0.9	394.8 ± 48.2	Mooy et al.
Chaetoceros affinis	10.5 ± 3.6	26.3 ± 9.0	Mooy et al.
Phaeodactylum tricornutum	1.1 ± 0.2	2.8 ± 0.4	This work

levels observed during the phosphate-limited phase, indicating depleted extracellular phosphorus and re-entry into the phosphorus-limited phase.

During the P or N limitation and depletion phases of a batch culture of the diatom *P. tricornutum*, the accumulation of TEPs was observed. A similar collection in response to N or P deficiency was found in a study on *Cylindrotheca closterium* (Staats et al., 2000). TEPs, originating from microorganisms, particularly phytoplankton (Alldredge et al., 1993), exhibit high viscosity and can adhere to phytoplankton cells, forming aggregates (Passow, 2002; Simon et al., 2002; Bar-Zeev et al., 2011). This phenomenon is supported by changes in overall cell morphology observed in this study. Large aggregates significantly contribute to vertical carbon flux and are considered a key factor driving the downward flux of particulate organic carbon. However, due to their lower density compared to seawater, TEPs tend to remain in surface waters in the absence of ballasting by other particles and can even move upward (Mari et al., 2017). In the nitrate depletion and spike experiments, as the concentration of TEPs increased, the settling rate of *P. tricornutum* decreased, indicating a significant negative correlation between TEPs concentration and sinking rate ($R = -0.71$, $P < 0.05$).

Distinct cellular contents were also observed under P-depleted and N-depleted conditions. In P-depleted cells, protein biosynthesis was suppressed, possibly related to the inhibition of nitrogen uptake (Alipanah et al., 2018). These results align with a previous study on P deficiency in *Aureococcus anophagefferens* (Wurch et al., 2011). In N-depleted cells, intracellular carbohydrates were accumulated. Huang et al. also reported the accumulation of carbohydrates within *Microcystis* under nitrogen limitation (Huang et al., 2019).

Despite their small particle size (< 20 μm) and the absence of frustules in the fusiform and triradiate forms, *P. tricornutum* exhibited a faster sinking rate under phosphorus-depleted conditions compared to *Skeletonema costatum*, *Ditylum brightwellii*, and *Chaetoceros gracile* (Bienfang et al., 1982). Rapid sinking is highly efficient in transporting particulate organic carbon to greater depths (Passow and Carlson, 2012). *P. tricornutum* is predominantly found in near-coastal areas, including estuaries (Martino et al., 2007), where currents converge or impinge on shelf margins, resulting in highly spatially and temporally variable nutrient concentrations and P-limited dominance in summer, such as in the Yangtze and Pearl River estuaries (Wong et al., 1998; Xu et al., 2008). The ability to rapidly respond to changes in nutrient concentrations may be particularly advantageous for *P. tricornutum* to exploit patchy nutrient distributions, contributing significantly to carbon export under P-limited conditions.

Data availability statement

The original contributions presented in the study are included in the article/Supplementary Material. Further inquiries can be directed to the corresponding author.

Author contributions

WZ: Conceptualization, Supervision, Data curation, Formal Analysis, Investigation, Methodology, Software, Validation, Writing – original draft, Writing – review & editing. QH: Conceptualization, Funding acquisition, Methodology, Resources, Supervision, Writing – review & editing. JZ: Data curation, Software, Formal Analysis, Validation, Writing – review & editing. YD: Data curation, Methodology, Software, Writing – review & editing. MX: Data curation, Software, Writing – review & editing. YC: Funding acquisition, Project administration, Supervision, Writing – review & editing. CL: Methodology, Project administration, Supervision, Validation, Writing – review & editing. HZ: Methodology, Project administration, Software, Validation, Writing – review & editing. FL: Funding acquisition, Project administration, Resources, Validation, Writing – review & editing.

Funding

The author(s) declare financial support was received for the research, authorship, and/or publication of this article. This study was funded by the Open Foundation of Donghai Laboratory (Grant No. DH-2022KF0215), the Impact and Response of Antarctic Seas to Climate Change Project (IRASCC 01-02-01A), the Zhejiang Provincial Ten Thousand Talents Plan (Grant No. 2020R52038), and the United Nations Ocean Decade Project of "The Exchange Between Kuroshio and Marginal Sea and Its Ecological Effect".

Conflict of interest

The authors declare that the research was conducted in the absence of any commercial or financial relationships that could be construed as a potential conflict of interest.

Publisher's note

All claims expressed in this article are solely those of the authors and do not necessarily represent those of their affiliated organizations, or those of the publisher, the editors and the reviewers. Any product that may be evaluated in this article, or claim that may be made by its manufacturer, is not guaranteed or endorsed by the publisher.

Supplementary material

The Supplementary Material for this article can be found online at: https://www.frontiersin.org/articles/10.3389/fmars.2023.1255915/full#supplementary-material

References

Alipanah, L., Winge, P., Rohloff, J., Najafi, J., Brembu, T., and Bones, A. M. (2018). Molecular adaptations to phosphorus deprivation and comparison with nitrogen deprivation responses in the diatom Phaeodactylum tricornutum. *PloS One* 13 (2), e0193335. doi: 10.1371/journal.pone.0193335

Alldredge, A. L., Passow, U., and Logan, B. E. (1993). The abundance and significance of a class of large, transparent organic particles in the ocean. *Deep Sea Res. Part I: Oceanographic Res. Papers* 40 (6), 1131–1140. doi: 10.1016/0967-0637(93)90129-Q

Anderson, L. W. J., and Sweeney, B. M. (1977). Diel changes in sedimentation characteristics of Ditylum brightwelli: Changes in cellular lipid and effects of respiratory inhibitors and ion-transport modifiers 1. *Limnology Oceanography* 22 (3), 539–552. doi: 10.4319/lo.1977.22.3.0539

Anderson, L. W. J., and Sweeney, B. M. (1978). ROLE OF INORGANIC IONS IN CONTROLLING SEDIMENTATION RATE OF A MARINE CENTRIC DIATOM DITYLUM BRIGHTWELLI1,2. *J. Phycology* 14 (2), 204–214. doi: 10.1111/j.1529-8817.1978.tb02450.x

Bar-Zeev, E., Berman, T., Rahav, E., Dishon, G., Herut, B., Kress, N., et al. (2011). Transparent exopolymer particle (TEP) dynamics in the eastern Mediterranean Sea. *Mar. Ecol. Prog. Ser.* 431, 107–118. doi: 10.3354/meps09110

Bienfang, P. K. (1981). Sinking rates of heterogeneous, temperate phytoplankton populations. *J. Plankton Res.* 3 (2), 235–253. doi: 10.1093/plankt/3.2.235

Bienfang, P. K., Harrison, P. J., and Quarmby, L. M. (1982). Sinking rate response to depletion of nitrate, phosphate and silicate in four marine diatoms. *Mar. Biol.* 67 (3), 295–302. doi: 10.1007/BF00397670

Bienfang, P., and Szyper, J. (1982). Effects of temperature and salinity on sinking rates of the centric diatom Ditylum brightwelli. *Biol. Oceanography* 1 (3), 211–223. doi: 10.1080/01965581.1982.10749440

Boudière, L., Michaud, M., Petroutsos, D., Rébeillé, F., Falconet, D., Bastien, O., et al. (2014). Glycerolipids in photosynthesis: Composition, synthesis and trafficking. *Biochim. Biophys. Acta (BBA) - Bioenergetics* 1837 (4), 470–480. doi: 10.1016/j.bbabio.2013.09.007

Boyd, C., and Gradmann, D. (2002). Impact of osmolytes on buoyancy of marine phytoplankton. *Mar. Biol.* 141 (4), 605–618. doi: 10.1007/s00227-002-0872-z

Boyd, P., and Newton, P. (1995). Evidence of the potential influence of planktonic community structure on the interannual variability of particulate organic carbon flux. *Deep Sea Res. Part I: Oceanographic Res. Papers* 42 (5), 619–639. doi: 10.1016/0967-0637(95)00017-Z

Buck, K., Chavez, F., and Davis, A. (2008). Minidiscus trioculatus, a small diatom with a large presence in the upwelling systems of central California. *Nova Hedwigia Beihefte* 133, 1.

Cai, Z., Duan, S., and Wei, W. (2009). Darkness and UV radiation provoked compensatory growth in marine phytoplankton Phaeodactylum tricornutum (Bacillariophyceae). *Aquaculture Res.* 40 (13), 1559–1562. doi: 10.1111/j.1365-2109.2009.02218.x

Canovas, S., Picot, B., Casellas, C., Zulkifi, H., Dubois, A., and Bontoux, J. (1996). Seasonal development of phytoplankton and zooplankton in a high-rate algal pond. *Water Sci. Technol.* 33 (7), 199–206. doi: 10.2166/wst.1996.0139

Caspers, H. (1970). *A Practical Handbook of Seawater Analysis* Vol. 167. Eds. J. D. H. Strickland and T. R. Parsons (Ottawa: Fisheries Research Board of Canada, Bulletin), 1968.

Chen, Y., Liu, R., Sun, C., Zhang, P., Feng, C., and Shen, Z. (2012). Spatial and temporal variations in nitrogen and phosphorous nutrients in the Yangtze River Estuary. *Mar. pollut. Bull.* 64 (10), 2083–2089. doi: 10.1016/j.marpolbul.2012.07.020

Daniels, C. J., Poulton, A. J., Esposito, M., Paulsen, M. L., Bellerby, R., St John, M., et al. (2015). Phytoplankton dynamics in contrasting early stage North Atlantic spring blooms: composition, succession, and potential drivers. *Biogeosciences* 12 (8), 2395–2409. doi: 10.5194/bg-12-2395-2015

Du Clos, K. T., Karp-Boss, L., and Gemmell, B. J. (2021). Diatoms rapidly alter sinking behavior in response to changing nutrient concentrations. *Limnology Oceanography* 66 (3), 892–900. doi: 10.1002/lno.11649

Du Clos, K. T., Karp-Boss, L., Villareal, T. A., and Gemmell, B. J. (2019). Coscinodiscus wailesii mutes unsteady sinking in dark conditions. *Biol. Lett.* 15 (3), 20180816. doi: 10.1098/rsbl.2018.0816

Field, C. B., Behrenfeld, M. J., Randerson, J. T., and Falkowski, P. (1998). Primary production of the biosphere: integrating terrestrial and oceanic components. *Science* 281 (5374), 237–240. doi: 10.1126/science.281.5374.237

Gemmell, B. J., Oh, G., Buskey, E. J., and Villareal, T. A. (2016). Dynamic sinking behaviour in marine phytoplankton: rapid changes in buoyancy may aid in nutrient uptake. *Proc. R. Soc. B: Biol. Sci.* 283 (1840), 20161126. doi: 10.1098/rspb.2016.1126

Gould, J. R.W., and Wiesenburg, D. A. (1990). Single-species dominance in a subsurface phytoplankton concentration at a Mediterranean Sea front. *Limnology Oceanography* 35 (1), 211–219. doi: 10.4319/lo.1990.35.1.0211

Granata, T. C. (1991). Diel periodicity in growth and sinking rates of the centric diatom Coscinodiscus concinnus. *Limnology Oceanography* 36 (1), 132–139. doi: 10.4319/lo.1991.36.1.0132

Guillard, R. R., and Ryther, J. H. (1962). Studies of marine planktonic diatoms. I. Cyclotella nana Hustedt, and Detonula confervacea (cleve) Gran. *Can. J. Microbiol.* 8, 229–239. doi: 10.1139/m62-029

Holman, W. I. M. (1943). A new technique for the determination of phosphorus by the molybdenum blue method. *Biochem. J.* 37 (2), 256–259. doi: 10.1042/bj0370256

Huang, Y., Hong, J., Liang, C., Li, G., Shen, L., Zhang, H., et al. (2019). Nitrogen limitation affects the sinking property of Microcystis by promoting carbohydrate accumulation. *Chemosphere* 221, 665–671. doi: 10.1016/j.chemosphere.2019.01.080

Jin, X., Gruber, N., Dunne, J., Sarmiento, J. L., and Armstrong, R. (2006). Diagnosing the contribution of phytoplankton functional groups to the production and export of particulate organic carbon, CaCO3, and opal from global nutrient and alkalinity distributions. *Global Biogeochemical Cycles* 20 (2), GB2015. doi: 10.1029/2005GB002532

Johnson, M. B., and Wen, Z. (2009). Production of biodiesel fuel from the microalga schizochytrium limacinum by direct transesterification of algal biomass. *Energy Fuels* 23 (10), 5179–5183. doi: 10.1021/ef900704h

Laurentin, A., and Edwards, C. A. (2003). A microtiter modification of the anthrone-sulfuric acid colorimetric assay for glucose-based carbohydrates. *Anal. Biochem.* 315 (1), 143–145. doi: 10.1016/S0003-2697(02)00704-2

Lavoie, M., and Raven, J. A. (2020). How can large-celled diatoms rapidly modulate sinking rates episodically? *J. Exp. Bot.* 71 (12), 3386–3389. doi: 10.1093/jxb/eraa129

Lavoie, M., Raven, J. A., and Levasseur, M. (2016). Energy cost and putative benefits of cellular mechanisms modulating buoyancy in aflagellate marine phytoplankton. *J. Phycology* 52 (2), 239–251. doi: 10.1111/jpy.12390

Leblanc, K., Quéguiner, B., Diaz, F., Cornet, V., Michel-Rodriguez, M., Durrieu de Madron, X., et al. (2018). Nanoplanktonic diatoms are globally overlooked but play a role in spring blooms and carbon export. *Nat. Commun.* 9 (1), 953. doi: 10.1038/s41467-018-03376-9

Legendre, L., and Le FÃƒÂ¨vre, J. (1995). Microbial food webs and the export of biogenic carbon in oceans. *Aquat. Microbial Ecol.* 09 (1), 69–77. doi: 10.3354/ame009069

Lewin, J. C., Lewin, R., and Philpott, D. (1958). Observations on phaeodactylum tricornutum. *Microbiology* 18 (2), 418–426. doi: 10.1099/00221287-18-2-418

Liu, Y. Y., Shen, F., and Li, X. Z. (2015). Phytoplankton light absorption properties during the blooms in adjacent waters of the changjiang estuary. *Huan Jing Ke Xue* 36 (6), 2019–2027.

Liu, Z., Xu, P., Gong, F., Tan, Y., Han, J., Tian, L., et al. (2022). Altered lipidomic profiles in lung and serum of rat after sub-chronic exposure to ozone. *Sci. Total Environ.* 806, 150630. doi: 10.1016/j.scitotenv.2021.150630

Luke, C. L. (1953). Photometric determination of silicon in ferrous, ferromagnetic, nickel, and copper alloys: A molybdenum blue method. *Analytical Chem.* 25 (1), 148–151. doi: 10.1021/ac60073a028

Mari, X., Passow, U., Migon, C., Burd, A. B., and Legendre, L. (2017). Transparent exopolymer particles: Effects on carbon cycling in the ocean. *Prog. oceanography* 151, 13–37. doi: 10.1016/j.pocean.2016.11.002

Martino, A. D., Meichenin, A., Shi, J., Pan, K., and Bowler, C. (2007). Genetic and phenotypic characterization of Phaeodactylum tricornutum (Bacillariophyceae) accessions[1]. *J. Phycology* 43 (5), 992–1009. doi: 10.1111/j.1529-8817.2007.00384.x

Matyash, V., Liebisch, G., Kurzchalia, T. V., Shevchenko, A., and Schwudke, D. (2008). Lipid extraction by methyl-tert-butyl ether for high-throughput lipidomics. *J. Lipid Res.* 49 (5), 1137–1146. doi: 10.1194/jlr.D700041-JLR200

Orlowska, E., Roller, A., Pignitter, M., Jirsa, F., Krachler, R., Kandioller, W., et al. (2017). Synthetic iron complexes as models for natural iron-humic compounds: Synthesis, characterization and algal growth experiments. *Sci. Total Environ.* 577, 94–104. doi: 10.1016/j.scitotenv.2016.10.109

Osibanjo, O., and Ajayi, S. O. (1980). Rapid and sensitive spectrophotobetric method for the determination of nitrate in rain water using 3,4-xylenol. *Analyst* 105 (1254), 908–912. doi: 10.1039/an9800500908

Passow, U. (2002). Transparent exopolymer particles (TEP) in aquatic environments. *Prog. Oceanography* 55 (3-4), 287–333. doi: 10.1016/S0079-6611(02)00138-6

Passow, U., and Alldredge, A. L. (1995). A dye-binding assay for the spectrophotometric measurement of transparent exopolymer particles (TEP). *Limnology Oceanography* 40 (7), 1326–1335. doi: 10.4319/lo.1995.40.7.1326

Passow, U., and Carlson, C. A. (2012). The biological pump in a high CO_2 world. *Mar. Ecol. Prog. Ser.* 470, 249–271. doi: 10.3354/meps09985

Raven, J. A., and Doblin, M. A. (2014). Active water transport in unicellular algae: where, why, and how. *J. Exp. Bot.* 65 (22), 6279–6292. doi: 10.1093/jxb/eru360

Simon, M., Grossart, H.-P., Schweitzer, B., and Ploug, H. (2002). Microbial ecology of organic aggregates in aquatic ecosystems. *Aquat. Microbial Ecol.* 28 (2), 175–211. doi: 10.3354/ame028175

Smayda, T. J. (1970). The suspension and sinking of phytoplankton in the sea. *Oceanogr. Mar. Biol. Ann. Rev.* 8, 353–414.

Smetacek, V. (1999). Diatoms and the ocean carbon cycle. *Protist* 150 (1), 25–32. doi: 10.1016/S1434-4610(99)70006-4

Staats, N., Stal, L. J., and Mur, L. R. (2000). Exopolysaccharide production by the epipelic diatom Cylindrotheca closterium: effects of nutrient conditions. *J. Exp. Mar. Biol. Ecol.* 249 (1), 13–27. doi: 10.1016/S0022-0981(00)00166-0

Tarafder, P. K., and Rathore, D. P. S. (1988). Spectrophotometric determination of nitrite in water. *Analyst* 113 (7), 1073–1076. doi: 10.1039/an9881301073

Tréguer, P., Bowler, C., Moriceau, B., Dutkiewicz, S., Gehlen, M., Aumont, O., et al. (2018). Influence of diatom diversity on the ocean biological carbon pump. *Nat. Geosci.* 11 (1), 27–37. doi: 10.1038/s41561-017-0028-x

Turner, J. T. (2015). Zooplankton fecal pellets, marine snow, phytodetritus and the ocean's biological pump. *Prog. Oceanography* 130, 205–248. doi: 10.1016/j.pocean.2014.08.005

Van Mooy, B. A., Fredricks, H. F., Pedler, B. E., Dyhrman, S. T., Karl, D. M., Koblížek, M., et al. (2009). Phytoplankton in the ocean use non-phosphorus lipids in response to phosphorus scarcity. *Nature* 458 (7234), 69–72. doi: 10.1038/nature07659

Waterborg, J. H. (2009). "The lowry method for protein quantitation," in *The Protein Protocols Handbook*. Ed. J. M. Walker (Totowa, NJ: Humana Press), 7–10.

Wong, G., Gong, G.-C., Liu, K., and Pai, S. (1998). 'Excess nitrate'in the east China sea. *Estuarine Coast. Shelf Sci.* 46 (3), 411–418. doi: 10.1006/ecss.1997.0287

Wurch, L. L., Haley, S. T., Orchard, E. D., Gobler, C. J., and Dyhrman, S. T. (2011). Nutrient-regulated transcriptional responses in the brown tide-forming alga Aureococcus anophagefferens. *Environ. Microbiol.* 13 (2), 468–481. doi: 10.1111/j.1462-2920.2010.02351.x

Xu, J., Yin, K., He, L., Yuan, X., Ho, A. Y., and Harrison, P. J. (2008). Phosphorus limitation in the northern South China Sea during late summer: influence of the Pearl River. *Deep Sea Res. Part I: Oceanographic Res. Papers* 55 (10), 1330–1342. doi: 10.1016/j.dsr.2008.05.007

Xue, Q., Wang, R., Xu, W., Wang, J., and Tan, L. (2018). The stresses of allelochemicals isolated from culture solution of diatom Phaeodactylum tricornutum Bohlin on growth and physiology of two marine algae. *Aquat. Toxicol.* 205, 51–57. doi: 10.1016/j.aquatox.2018.10.004